The Contaminate Infiltration Model for Heat and Concentration Transport Within Porous Media Under Electromagnetic Fields

Prempreeya Montienthong
Department of Sustainable Development Technology,
Faculty of Science and Technology,
Thammasat University (Rangsit Campus),
Pathumthani 12120, Thailand
e-mails: prempree@tu.ac.th;
monprempreeya@gmail.com

Phadungsak Rattanadecho[1]
Center of Excellence in Electromagnetic Energy Utilization in Engineering (CEEE),
Department of Mechanical Engineering,
Faculty of Engineering,
Thammasat University (Rangsit Campus),
Pathumthani 12120, Thailand
e-mail: ratphadu@engr.tu.ac.th

Andy Gibson
Faculty of Science and Engineering,
Manchester Metropolitan University,
All Saints Building, All Saints,
Manchester M15 6BH, UK

This paper studies the groundwater model of the influence of physical parameters, including input frequency of the electromagnetic, and input concentration of contaminants in groundwater, on the velocity pattern, temperature distribution, and concentration distribution of convective heat transfer in saturated porous media as soil. The mathematical models have solved seven equations in this simulation study, i.e., Maxwell's equation, heat transfer in fluid and solid phases, momentum, and concentration equations. The effect of frequencies and input concentrations of contaminants on the convective heat transfer and concentration distribution in porous media as soil under an electromagnetic wave is investigated. The results indicate that the electromagnetic wave frequency of 2.45 GHz has the most influence on the temperature distribution, velocity patterns, and concentration distribution of the fluid within the porous media as soil during saturated flow in groundwater. The inlet fluid concentration of the contaminant at 30 mol/dm^3 has the most impact on the temperature distribution between the implementation of an electromagnetic wave of 2.45 GHz. So, this numerical model provides simple decision data based on comparing the maximum contaminant concentrations of porous media as soil samples with surface soil screening levels such as petroleum engineering and agricultural engineering. This result can be used by the engineer as a guide to determine whether further investigation is needed. [DOI: 10.1115/1.4055762]

Keywords: concentration of contaminant transport in soil, contamination of groundwater, electromagnetic fields, Darcy–Brinkman–Forchheimer's model, local thermal non equilibrium models, LTNE models

1 Introduction

Groundwater is fresh water that permeates into the soil and is stored in the pores in the middle of rocks and particles of soil. It is stored in the little open spaces between rock, sand, soil, and gravel. Groundwater is a significant resource for human and living things' survival. Furthermore, it is also important to partake in industrial progress. Contamination of groundwater has emerged as a major environmental issue, particularly in light of the current increase in energy demand and instrumentality evolution. As a result, environmentalists and engineers are exceedingly faced with the complicated job of planning waste management to eliminate the contamination of groundwater for simplicity. To manage the problem, they had to implement processes that handle the transport of contaminants. In particular, heat and concentration transport of electromagnetic during saturated flow in porous media such as soil and alkaline soil, etc.

Modern technology has widely developed using energy systems, of which the most relevant is certainly electricity or electromagnetic fields. The electromagnetic has been a heat source, which is rather more fascinating than the conventional heating processes used in common industry. The electromagnetic can infiltrate the soil full of water and shift to become thermal energy fast within the soil. A lot of electromagnetic energy has been used in various industrial applications. Applications involving heat-generating electromagnetics are universally accomplished in the food industry and packaging in the microwave oven, such as drying processes, pasteurization, and sterilization [1]. In addition, home devices that work using diversified current expose humans to electromagnetic fields. Moreover, the trams, trains, and electric trains also generate a magnetic field that penetrates the soil.

As mentioned above, electromagnetic fields produce radiation, which causes the so-called electromagnetic wave pollution that spreads to the environment. Water motion in underground augmentation of chemical waste, geothermal reservoirs, evaporative cooling, thermal insulation, and solidification [2,3] was discovered to merge with natural convection heat in porous media. Furthermore, the study of swirling flow in a duct under the electrohydrodynamic using the Coulomb force term and the Navier–Stokes equation was studied by Saneewong Na Ayuttaya et al. [4]. The results showed the distributions of the electric field from varied ground arrangements are different and the characteristics of swirling flow are shown differently.

Soil is one of the porous media. Porous soil genres consist of rough particles which lose large areas known as pores, or the areas between the particles of silt, sand, and clay that make up the structure of soil, which is to hold air and water. The volume of water it can hold, and the volume of rapid water draining out of the soil, is related to the size and number of pores in the soil. Nevertheless, this paper studied saturated porous media—the space or void of soil is full of water.

Diffusion is responsible for mass transfer, which is the movement of a molecule from an area of higher concentration to an area of lower concentration until equilibrium is reached. It is always found in routine life; for example, the pollutants or

[1]Corresponding author.

Contributed by the Heat Transfer Division of ASME for publication in the Journal of Heat and Mass Transfer. Manuscript received May 10, 2022; final manuscript received August 18, 2022; published online December 9, 2022. Assoc. Editor: Yogesh Jaluria.

contamination of groundwater are included. Pengpom et al. [5] studied a part of the Chao Phraya River in Thailand for pollution and temperature. The results show that an escalation in the inlet velocities of both canals is increasing pollutants.

Natural convection on porous media, heat, mass transport, and double-diffusive convection flow were all investigated [6–8]. Trevisan and Bejan [7] presented the mass transfer when the buoyancy effect was due entirely to the temperature.

Heat and mass transfers in the freezing processes and microwave heating, which comprises natural convection in the fluid phase and porous media, were studied for many years. References [9–18], show that mass and heat phenomena in porous media are more complicated than in fluids. Yousefi et al. [11] researched the influence of microwave heating under unremitting water flow in a pipe. They developed a model on ANSYS MULTIPHYSICS that operates at a 915 MHz frequency to compute the temperature change in water flow. Numerical results show that if inlet velocity increases, the average outlet temperature decreases. Moreover, the applicator size is raised more than the critical value, which will affect heat absorption that drops significantly.

The local thermal equilibrium (LTE) model will consider the solid temperature as the fluid temperature phase throughout the porous media. Nevertheless, this temperature difference between fluids and solids has an essential influence on the heat process, which affects many physical properties in the soil. Therefore, in this study, the local thermal non equilibrium (LTNE) models has been brought to analyze the temperature distribution, velocity, and concentration in the groundwater model under electromagnetic field.

Heat transfer and natural convection in porous media or biomaterials were investigated [19–29]. Previous studies focused on studies that were applied to biological materials, such as Belmiloudi [19] and Afrin et al. [20]. They studied biofluid heat transfer about the temperature between thermal therapy and a thermal lagging model in living biological tissue within the tissue, venous and arterial by the LTNE model.

The study involves several applications, including geophysics. Examples of past research include the flow in a two-dimensional inclined channel with a porous layer saturated with a viscous fluid and a second layer with a clear viscous fluid under the influence of electromagnetic force. The injection velocity, the saturation transition zone, and the sloped incoming groundwater flow are all affected. Furthermore, a theoretical model for CO_2 migration in tilted aquifers with groundwater flow is presented. The capacity of reservoirs and the migration process were studied [30,31]. Moreover, it includes the infiltration of beauty cream into the layer of skin that is used in medical applications.

The objectives of this study were to develop a mathematical model in a case study about the flow of contaminants through porous media by solving seven equations, namely, Maxwell's equations, continuity equation, momentum equations (x, y), energy equation of fluid and solid phase, and the last one, the concentration equation, to determine the concentration distribution, temperature distribution, and flow pattern of groundwater within a porous media as the soil under the electromagnetic energy by the LTNE model. This study used numerical analysis at a varied electromagnetic frequency and varied input concentrations. Moreover, the transient energy terms in the two-phases, concentration, and momentum equations were analyzed together with Maxwell's equation.

This is a novelty in this work that describes the phenomenon of contamination of groundwater such that the flow of fluid across the permeable media is of tremendous interest. Fluid dynamics specialists and geophysicists are interested in this kind of flow. Their uses span a wide range of industries. Some are in petroleum engineering and environmental engineering, where it's crucial to observe the flow of natural gas and oil via reservoirs, while others are in agricultural engineering, where academics talk about groundwater supplies and leakage contaminants. Moreover, this phenomenon is also involved in the refinement, cleaning, and substrate removal processes in chemical engineering, i.e., investigating chemical substrate removal using a multilayer mass transfer system in a reactor made of granular activated carbon (GAC) covered with biofilm, etc. [32]

2 Modeling and Formulation

The physical domains of the problem and view of unsaturated soil were displayed in Figs. 1(*a*) and 1(*b*), respectively. The physical domain was analyzed for heat and contaminant transport and fluid flow in porous media as soil exposed to electromagnetic waves.

The 2D schematic diagram present in Fig. 1(*c*) is comprised of porous media as soil that was filled within the rectangular waveguide. The waveguide walls were assumed to be made of a metal that anticipates a perfect electrical conductor. This study analyzes the fundamental mode (TE_{10}) monochromic wave. The domain where the electromagnetic wave is diagnosed includes all areas besieged by the waveguide walls. Flow and temperature patterns are restricted to the region besieged by the rectangular waveguide [3].

This study presents the essential aspects for a fundamental understanding of saturated flow and distributed concentration in porous media such as soil, between receiving electromagnetic signals. Table 1 shows how this study used the thermal and dielectric properties of soda lime, air, and contaminated water for porous media as soil in computing.

2.1 The Electromagnetic Field Analysis. TE_{10} mode of Maxwell's equations was modified to get the electromagnetic wave in a rectangular waveguide in porous media [9]

$$E_z, H_x, H_y \neq 0 \tag{1}$$

$$\frac{\partial E_z}{\partial t} = \frac{1}{\gamma}\left(\frac{\partial H_y}{\partial x} - \frac{\partial H_x}{\partial y} - \sigma E_z\right) \tag{2}$$

$$\frac{\partial H_x}{\partial t} = -\frac{1}{\varphi}\left(\frac{\partial E_z}{\partial y}\right) \tag{3}$$

$$\frac{\partial H_y}{\partial t} = \frac{1}{\varphi}\left(\frac{\partial E_z}{\partial x}\right) \tag{4}$$

where H is the magnetic field (A/m), E is the electric field (V/m), γ is electric permittivity, φ is magnetic permeability, and σ is electric conductivity (S m^{-1}).

Boundary conditions:

(1) At walls, the perfect conduction condition, the regular constitutive of the magnetic field, and the tangential constitutive of the electric field vanish [9]

$$H_n = 0, \quad E_t = 0 \tag{5}$$

t denotes the direction of the tangential component, and n denotes the direction of the normal component.

(2) The first order absorbing condition by Mur [33] is at the edge of the waveguide

$$\frac{\partial E_x}{\partial t} = \pm c\frac{\partial E_x}{\partial x} \tag{6}$$

The symbol ±demonstrates forward and backward directions.

The wave's velocity is given by c.

(3) The equations are used to simulate electromagnetic waves [9]

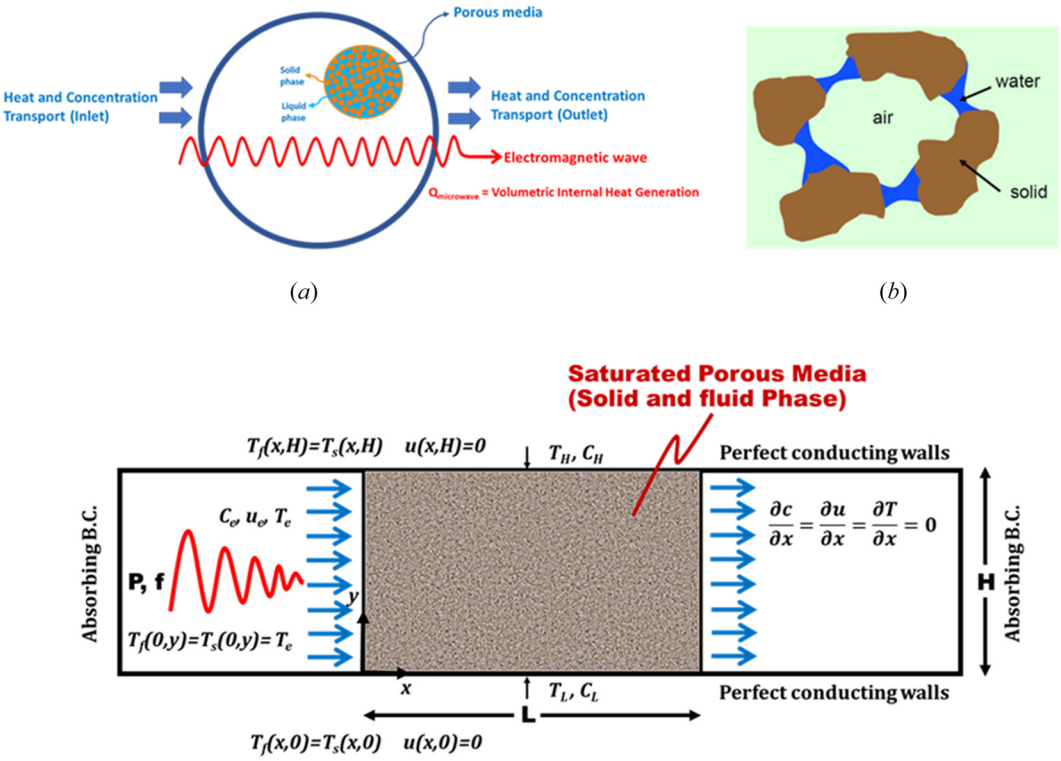

Fig. 1 Computational model (*a*) the physical domains of the problem, (*b*) view of unsaturated soil (ref: the following footnote link[2]), and (*c*) the 2D schematic diagram

Table 1 The thermal and dielectric properties of the model [21]

Material property	Air	Water	Soda lime
Density, ρ $(\mathrm{kg/m^3})$	1.1	989	2225
Specific heat, C_p $(J\,\mathrm{kg^{-1}K^{-1}})$	1008	4180	835
Thermal conductivity, k $(\mathrm{Wm^{-1}K^{-1}})$	0.028	0.640	1.4
Viscosity, μ $(\mathrm{kgm^{-1}s^{-1}})\times 10^5$	1.9	57.7	—
Dielectric constant, γ_r	1.0	$88.15-0.414T+(0.131\times10^{-2})T^2-(0.046\times10^{-4})T^3$	7.5
Loss tangent, tan δ	0.0	$0.323-(9.499\times10^{-3})T+(1.27\times10^{-4})T^2-(6.13\times10^{-7})T^3$	0.0125

$$E_z = E_{zin}\sin\left(\frac{\pi y}{a}\right)\sin(2\pi ft) \tag{7}$$

$$H_y = \frac{E_{zin}}{Z_H}\sin\left(\frac{\pi y}{a}\right)\sin(2\pi ft) \tag{8}$$

where f is the frequency (GHz) of an electromagnetic wave, y is the width of the rectangular waveguide, Z_H is the wave impedance, E_{zin} is the operating input of the electric field intensity. E_{zin} is appraised by the operating power input of the electromagnetic wave that applies the Poynting theorem

$$E_{zin} = \sqrt{\frac{4Z_H P_{in}}{A}} \tag{9}$$

P_{in} is the operating input electromagnetic wave power and A is the incident plane area.

(4) The interfaces between different materials use the continuity conditions as

$$E_t = E_t', \quad H_t = H_t' \tag{10}$$

$$D_n = D_n', \quad B_n = B_n' \tag{11}$$

Initial condition

$$E, H = 0; \quad t = 0 \tag{12}$$

2.2 Analysis of Flow Pattern, Temperature Distribution, and Concentration of Contaminant. To abbreviate the sophistication of the analysis of flow pattern, temperature distribution, and concentration of contaminant, the following assumptions are applicable: that the fluid has no phase change emerges, the fluid is an incompressible fluid, the Boussinesq approximation is useable, the porous media is isotropic, the effect of the magnetic field on heating is futile, and thermal dispersion is forsaken.

The equations for estimation of the velocity pattern and heat transfer.

Continuity equation and momentum equation on x–y axis [34]

$$\frac{\partial u}{\partial x}+\frac{\partial v}{\partial y}=0 \tag{13}$$

$$\frac{1}{\varepsilon}\left(\frac{\partial u}{\partial t}\right)+\frac{1}{\varepsilon^2}\left(u\frac{\partial u}{\partial x}+v\frac{\partial u}{\partial y}\right)=-\frac{1}{\rho_f}\left(\frac{\partial p}{\partial x}\right)+\frac{\mu}{\varepsilon}\left(\frac{\partial^2 u}{\partial x^2}+\frac{\partial^2 u}{\partial y^2}\right)-\frac{\mu u}{\kappa}-\frac{F\mu}{\sqrt{\kappa}}(u^2+v^2)^{\frac{1}{2}}u \tag{14}$$

[2]https://ocw.mit.edu

$$\frac{1}{\varepsilon}\left(\frac{\partial v}{\partial t}\right)+\frac{1}{\varepsilon^2}\left(u\frac{\partial v}{\partial x}+v\frac{\partial v}{\partial y}\right)=-\frac{1}{\rho_f}\left(\frac{\partial p}{\partial y}\right)+\frac{\mu}{\varepsilon}\left(\frac{\partial^2 v}{\partial x^2}+\frac{\partial^2 v}{\partial y^2}\right)-\frac{\mu v}{\kappa}-\frac{F\mu}{\sqrt{\kappa}}(u^2+v^2)^{\frac{1}{2}}v+g\beta_T(T-T_0)+g\beta_C(C-C_0) \tag{15}$$

where β_T and β_C are coefficient of thermal expansion and coefficient of concentration expansion, respectively.

The geometric function, F and permeability, κ [21]

$$F=\frac{1.75}{\sqrt{150\varepsilon^3}} \tag{16}$$

$$\kappa=\frac{\varepsilon^3 d_p^2}{150(1-\varepsilon)^2} \tag{17}$$

The variation of porosity near the impermeable boundaries was expressed in this equation [21]

$$\varepsilon=\varepsilon_\infty\left[1+a_1\exp\left(-\frac{a_2 y}{d_p}\right)\right] \tag{18}$$

where ε_∞, is the freestream porosity, $a_1=1.7$ and $a_2=6$ are empirical constants. The free steam porosity is 0.37. The values were determined to be an excellent estimate of the experimental data [23]. The penetration depth was used to represent the depth in which the density of power decreased to 37% of its initial value on the surface [14]

$$D_p=\frac{1}{\frac{2\pi f}{\vartheta}\sqrt{\frac{\varepsilon_r'\left(\sqrt{1+\left(\frac{\varepsilon_r''}{\varepsilon_r'}\right)^2}-1\right)}{2}}}=\frac{1}{\frac{2\pi f}{\vartheta}\sqrt{\frac{\varepsilon_r'\sqrt{1+(\tan\delta)^2}-1}{2}}}$$

where D_p is penetration depth, ε_r'' is relative dielectric loss factor. And ϑ is electromagnetic wave speed. The penetration depth of the electromagnetic wave power was defined by this equation.

Fluid phase energy equation [34]

$$\varepsilon(\rho C_p)_f\frac{\partial T_f}{\partial t}+(\rho C_p)_f\left(u\frac{\partial T_f}{\partial x}+v\frac{\partial T_f}{\partial y}\right)=k_{f\text{eff}}\left(\frac{\partial^2 T_f}{\partial x^2}+\frac{\partial^2 T_f}{\partial y^2}\right)+h_{sf}a_{sf}(T_s-T_f)+\varepsilon Q_f \tag{19}$$

Solid phase energy equation [34]

$$(1-\varepsilon)(\rho C_p)_s\frac{\partial T_s}{\partial t}=k_{s\text{eff}}\left(\frac{\partial^2 T_s}{\partial x^2}+\frac{\partial^2 T_s}{\partial y^2}\right)-h_{sf}a_{sf}(T_s-T_f)+(1-\varepsilon)Q_s \tag{20}$$

where Q is the local electromagnetic heat generation term [9]

$$Q=2\pi f\gamma_0\gamma_r'(\tan\delta)\cdot(E_z)^2 \tag{21}$$

$$\tan\delta=\frac{\gamma_r''}{\gamma_r'}=\frac{\sigma}{\omega\gamma_r'\gamma_0} \tag{22}$$

where γ_0 is dielectric constant, γ_r' is relative dielectric constant, γ_r'' relative dielectric loss factor.

Concentration transport equation

$$\varepsilon\frac{\partial C}{\partial t}+u\frac{\partial C}{\partial x}+v\frac{\partial C}{\partial y}=D\left(\frac{\partial^2 C}{\partial x^2}+\frac{\partial^2 C}{\partial y^2}\right) \tag{23}$$

D is mass diffusivity, C is concentration (mol/dm^3), and t is time (s).

Boundary and initial conditions:

No-slip boundary conditions are applied at all walls. The boundary conditions are as follows:

$$T_f(0,y)=T_s(0,y)=T_e=27\,^\circ\text{C}$$

$$T_f(x,H)=T_s(x,H)=T_H=67\,^\circ\text{C}$$

$$T_f(x,0)=T_s(x,0)=T_L=15\,^\circ\text{C}$$

$$C(0,y)=C_e$$

$$C(x,H)=C_H=20\,\text{mol/dm}^3$$

$$C(x,0)=C_L=10\,\text{mol/dm}^3$$

$$u(0,y)=u_e,\text{Re}_p=\rho_f u_e d_p/\mu$$

Re_p is particle Reynold number, d_p is particle diameter (m), u_e is inlet velocity (m/s), and μ is viscosity of water = 57.7 kgm^{-1}s^{-1}

$$u(x,H)=0$$

$$u(x,0)=0$$

$$\text{Re}_p=0.1:\ u_e=1.17\times10^{-5}\,\text{m/s}$$

$$\text{Re}_p=0.5:\ u_e=5.83\times10^{-5}\,\text{m/s}$$

$$\text{Re}_p=10:\ u_e=1.17\times10^{-3}\,\text{m/s}$$

$$d_p=5.0\times10^{-3}\,\text{m}$$

Boundary conditions at the outlet are close to a fully developed condition

$$\frac{\partial C}{\partial x}=0,\quad \frac{\partial u}{\partial x}=0,\quad \frac{\partial T}{\partial x}=0$$

Initial conditions

$$T=T_0=27\,^\circ\text{C}$$

$$u=u_0$$

$$C=C_0=0\,\text{mol/dm}^3;\quad t=0$$

The thermal properties and dielectric properties were presented in Table 1 [21].

2.3 Calculation Procedure. Maxwell's equations were solved by the finite difference time-domain method. Equations (13)–(22) express the heat transport and fluid flow. The finite control volume approach with the SIMPLE algorithm is used to solve all equations that are coupled with Maxwell's equations. To approve the stability of the time-stepping algorithm, Δt is selected to fulfill the present stability condition.

$$\Delta t\le\frac{\sqrt{(\Delta x)^2+(\Delta y)^2}}{c} \tag{24}$$

$$\Delta x,\Delta y\le\frac{\lambda_g}{10\sqrt{\gamma_r}} \tag{25}$$

where λ_g is the wavelength of electromagnetic wave in the rectangular waveguide and γ_r is the relative electric permittivity. Grid size: $\Delta x = 1.0\,\text{mm}$ and $\Delta y = 1.0\,\text{mm}$. Time steps: $\Delta t = 2 \times 10^{-12}\,\text{s}$ was used consistent with electromagnetic field and $\Delta t = 0.01$ was used consistent with temperature distribution, velocity pattern, and concentration of contaminant computations. The relative error in the iteration procedures is assured less than 10^{-6}.

3 Results and Discussion

3.1 Verification of the Model. In the validation case which has an electromagnetic frequency of 2.45 GHz, electromagnetic power 1600 W, and Reynolds number (Re_p) is 0.1. The simple simulated result was validated against the result from the identical geometric model by Klinbun et al. [21]. Figure 2 shows the fluid phase temperature which clearly presents a good agreement of the fluid phase temperature values of the porous media between the present simulation and the work of Klinbun et al. This appropriate comparison lets reliability in the accuracy of the present numerical model and ensures which this model can exactly describe the heat transport phenomena in saturated porous media exposed to the electromagnetic wave.

3.2 Analysis of Electromagnetic Field. Figure 3(*a*) shows a result of an electric field distribution inside a rectangular waveguide when the porous packed bed as soil is inserted inside the guide at an electromagnetic wave frequency of 2.45 GHz, electromagnetic wave power of 500 W, particle Reynolds number ($\text{Re}_p = \rho_f u_e d_p/\mu) = 0.1$, and inlet concentration of contaminant 30 mol/dm^3, where the center of the porous media as soil can be seen which huge amplitude and slowly diminishes as the wave moves into the porous media as soil. Most waves are reflected back from the surface and demonstrate resonance with huge amplitude, while the electric field in the material slowly decreases and disappears because the wave is penetrated the porous media as soil.

Figure 3(*b*) shows a result of an electric field at varied electromagnetic wave frequencies (2.45, 4, 6, and 8 GHz), electromagnetic wave power of 1600 W, particle Reynolds number 0.1, and inlet concentration of contaminant 30 mol/dm^3. The results can describe the electric field distributions inside a rectangular waveguide when the porous packed bed is inserted in the waveguide at the frequency of 8 GHz which is a result of a transmitted wave at the incident face and a reflected wave from the lower surface of the porous media as soil. Also, electromagnetic wave operating at a high frequency has a short wavelength which corresponds to a smaller penetration depth of electromagnetic wave as compared with the depth of the porous media as soil. Therefore, the absorbed energy is converted to thermal energy, which increases the temperature of porous media as soil.

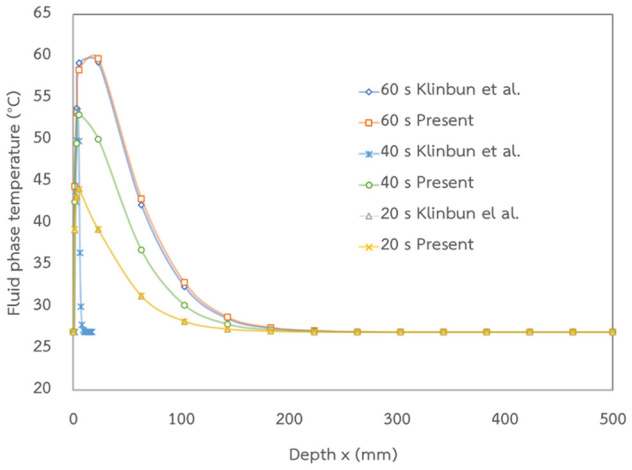

Fig. 2 The validation results of the calculated fluid phase temperature versus those obtained by Klinbun et al. [21]

3.3 The Influence of Frequency on the Temperature Distribution, Velocity Pattern, and Concentration of Contaminant in Porous Media

3.3.1 Distribution of Temperature. Figure 4 displays the effect of variations in the electromagnetic frequency on the distribution of temperature in fluid and solid phases at an operating electromagnetic wave power of 1600 W and varying electromagnetic wave frequencies of 2.45, 4, 6, and 8 GHz. The figure shows that the maximum elevated temperature values coincide with the lowest electromagnetic frequency. Moreover, at a frequency of 8 GHz, the extent of the temperature distribution is the lowest. Because of the electromagnetic frequency of 8 GHz, in this case, high-frequency waves have short wavelengths. And the depth of penetration is low. Waves are absorbed quickly at the side of the incident wave surface when the 8 GHz frequency of electromagnetic waves is compared to the 2.45 GHz frequency. Furthermore, Fig. 4 indicates the behavior of the temperature distribution that resembles a wave, which is not clear in the case of high frequencies. It is seen that the amplitude of the wave is relatively low, and the resonance of the standing wave seldom occurs. The phenomena of heat under the electromagnetic field are associated with the electromagnetic and the distribution of temperature. This study forecasts the electromagnetic, which indicates the force of the electromagnetic in dielectric materials like soil and also indicates that the power of the electromagnetic gently decreases. This means that the force of the electromagnetic is transformed into

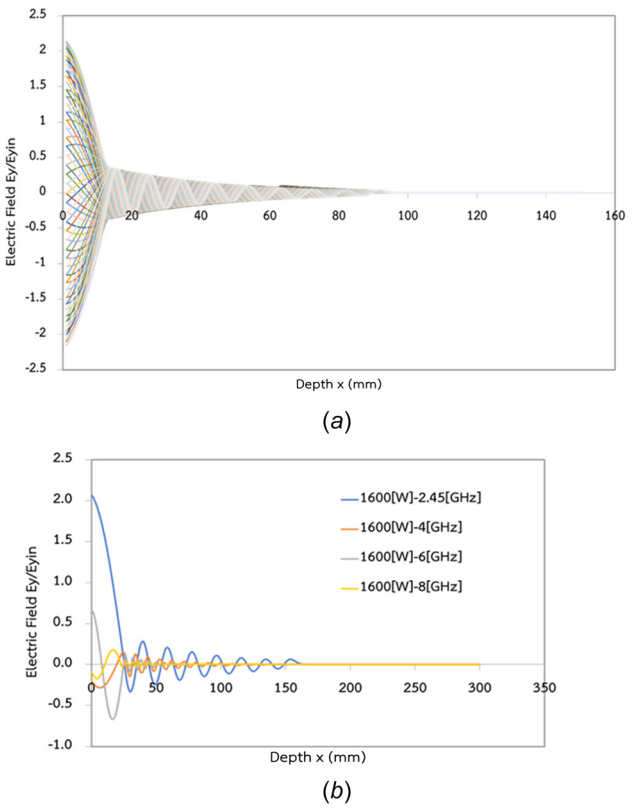

Fig. 3 Simulation of the electric field along the porous packed bed as soil on Reynolds number (Re_p) = 0.1, inlet concentration of contaminant (C_{in}) = 30 mol/dm^3: (*a*) electromagnetic wave frequency of 2.45 GHz, electromagnetic wave power of 500 W and (*b*) varied electromagnetic wave frequencies, electromagnetic wave power of 1600 W

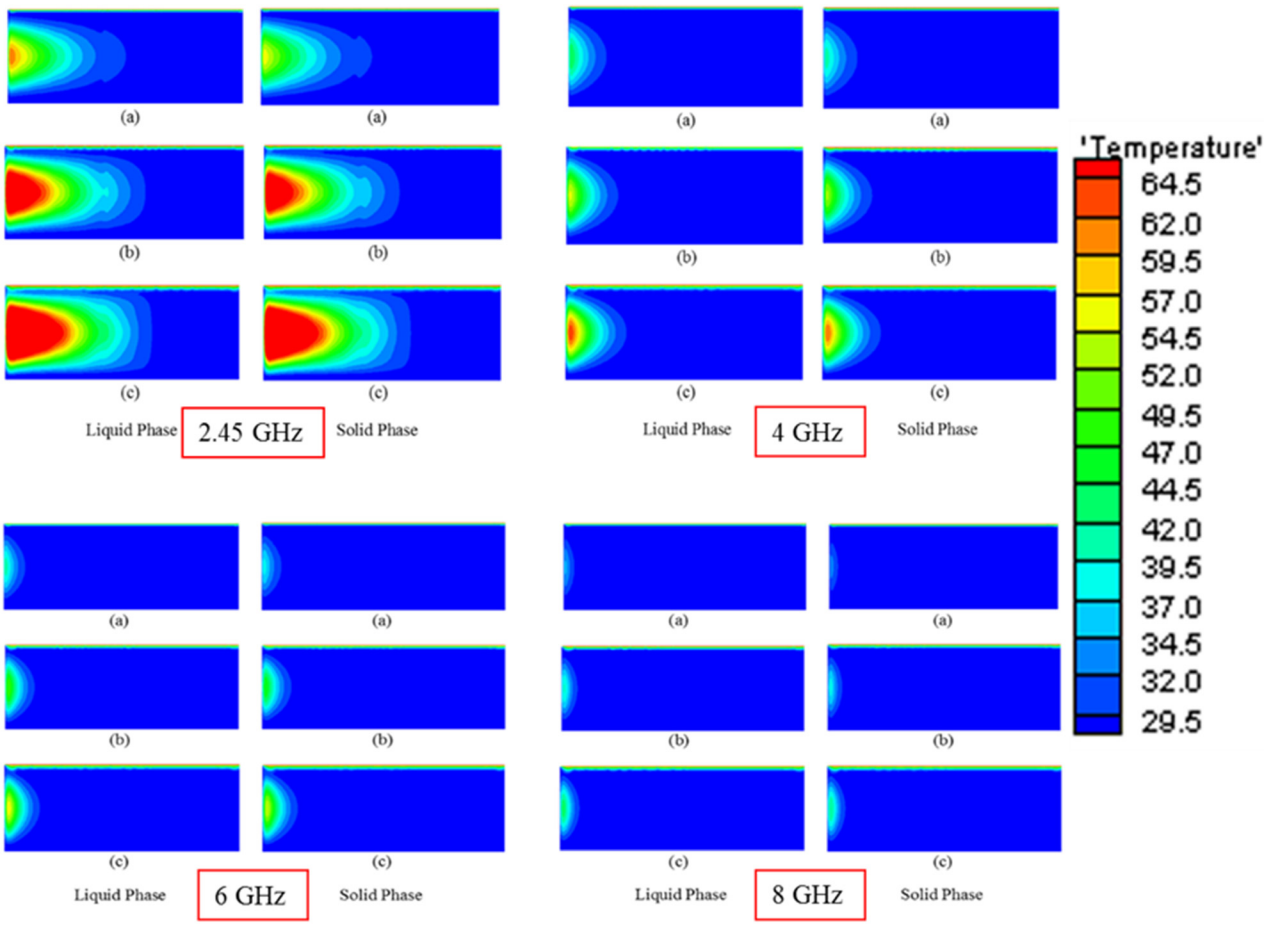

Fig. 4 The temperature distribution (°C) when elapsed times: (*a*) 20 s, (*b*) 40 s, and (*c*) 60 s at varied electromagnetic frequency operating electromagnetic power of 1600 W, Reynolds number (Re_p) = 0.1, inlet concentration of contaminant 30 mol/dm^3)

another, which is called heat. Therefore, the power of the electromagnetic wave decreases slightly as a result of dielectric materials such as soil which is absorbed where the wave has been changed into the heat form. This situation regards the internal heat generation in the porous media.

Figure 5(*a*) compares the percentage difference of the temperature distribution of the fluid and the solid phase during time 0–60 s on *x*-axis 25 and *y*-axis 99 mm. This comparison presents an electromagnetic power of 1600 W and varied electromagnetic frequencies of 2.45, 4, 6, and 8 GHz at the time of 10 s. It is the percentage difference of the distributions that is prominent at the electromagnetic frequency of 2.45 GHz (% LTE approximates 14). Consequently, this means the difference between fluid and solid phase will be greater than in the case of electromagnetic wave frequencies of 4, 6, and 8 GHz (% LTE approximate 1–7). In addition, the LTE assumption is not suitable in the case of an electromagnetic frequency of 2.45 GHz. It can be said that this simulation model is appropriate to use the LTNE assumption for the analysis.

The temperature distribution along the *x*-axis at position *y*-axis = 99 mm at 60 s at various inlet electromagnetic frequencies and electromagnetic wave power of 1600 W is shown in Fig. 5(*b*). The result indicates that the temperature increased and achieved the maximum at the *x*-axis at around 25 mm and then carefully decreased because of the electromagnetic. The temperature in the direction of the electromagnetic decreases; that means the electromagnetic energy has fluctuated to become heat energy, and the maximum temperature of the fluid phase is approximately 97, 63, 53, and 43 °C at values of electromagnetic frequencies of 2.45, 4, 6, and 8 GHz, respectively.

The temperature distribution along the *y*-axis at position *x*-axis = 25 mm at 60 s at various inlet electromagnetic frequencies with an electromagnetic wave power of 1600 W is shown in Fig. 5(*c*). This result indicates that the temperature escalated and achieved the maximum at the *y*-axis of around 99 mm, and then carefully reduced along the y-axis. The maximum temperatures of the fluid phase in the porous media as soil are approximately 93, 58, 46, and 33 °C at values of electromagnetic wave frequencies of 2.45, 4, 6, and 8 GHz, respectively. Finally, the temperature distribution turns to alleviate again and swings up on the upper boundary position because of the effect of boundary conditions, which result from the temperature and concentration that were defined in the upper region.

To categorize the percentage difference between the temperature distribution of the fluid and the solid phase, specifically in the following:

$$\%\text{LTE} = \left(\frac{T_{f(i,j)} - T_{s(i,j)}}{T_{f(i,j)}}\right) \times 100 \tag{26}$$

3.3.2 Velocity Patterns. Velocity patterns in the porous media as soil when the times 60 s are considered to indicate that the electromagnetic frequency has a significant impact on the velocity patterns in the porous media such as soil. This study case considers varied electromagnetic frequencies at 2.45, 4, 6, and 8 GHz

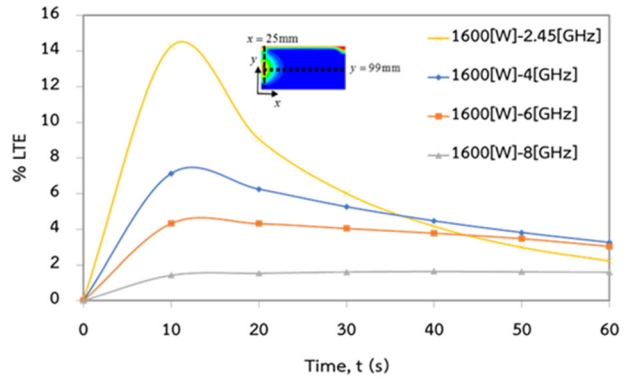

(*a*)

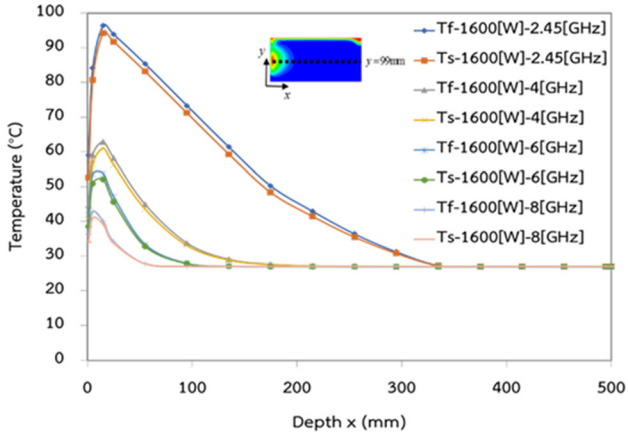

(*b*)

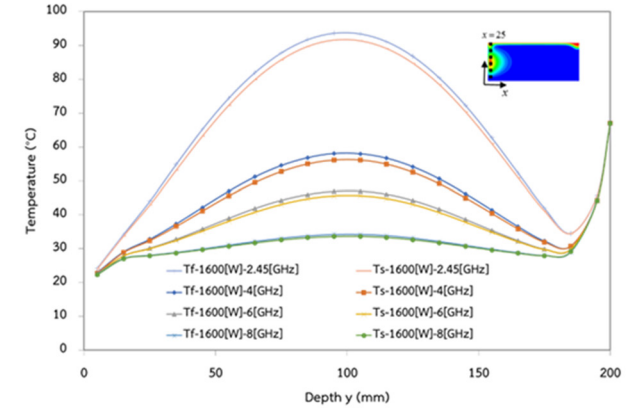

(*c*)

Fig. 5 Temperature distribution (electromagnetic power of 1600 W, inlet concentration of contaminant 30 mol/dm^3): (*a*) Percent difference of temperature distribution on solid and fluid phases at varied electromagnetic frequencies when elapsed times. (*b*) The temperature along *x*-axis at *y*-axis = 99 mm at 60 s (*c*) the temperature along *y*-axis at *x*-axis = 25 mm at 60 s.

when the electromagnetic power is 1600 W, $Re_p = 0.1$, and $C_{in} = 30$ mol/dm^3. Figure 6 indicates the velocity patterns internal to the porous media as soil when it was inserted into the waveguide between electromagnetic heating with varied frequencies. The results show that the magnitudes of fluid velocity patterns are obviously different in the case of an electromagnetic frequency of 2.45 GHz since the density of the electromagnetic in porous media is higher than in the case of an 8 GHz electromagnetic wave frequency, which is the maximum frequency in this study. However, the fluid velocity patterns are in the same direction. In addition, this figure indicates that the velocity pattern is violent close to the right corner of the top boundary of the porous media as soil because of the upper condition that defines the high temperature boundary condition and also indicates that velocity patterns have a trend consistent with the temperature distribution as already mentioned.

3.3.3 Distribution of Concentration. Figure 1(*c*) defined the upper boundary as a higher concentration than the lower boundary ($C_H = 20$ mol/dm^3, $C_L = 10$ mol/dm^3). The theory states that the diffusion of the concentration will expand from the high to the low concentration on porous media as soil. This study considers the diffusion of concentration from left to right when contaminate-containing fluid was fed on the left, exposing the electromagnetic. The concentration distribution in the porous media as soil when elapsed time is 60 s at varied electromagnetic frequencies of 2.45 and 4 GHz and electromagnetic power of 1600 W is listed in Table 2. The table indicates the electromagnetic frequency of 2.45 GHz, which is an overall higher distribution of concentration. For example, at 455 mm, the concentration of contaminants at the electromagnetic wave frequencies of 2.45 and 4 GHz is 9.00171 and 9.00127 mol/dm^3, respectively. This result is found with respect to the low electromagnetic wave frequency and high depth of penetration. In Table 2, the data for concentration was plotted on the bar graph shown in Fig. 7. The bar graph shows the trend of concentration distribution when elapsed time is 60 s along the *x*-axis at varied electromagnetic frequencies in the range of *y*-axis 199 mm, electromagnetic power 1600 w, and inlet concentration of contaminant 30 mol/dm^3. The determination of the boundary conditions at the upper surface of porous media as soil and fully developed flow results in the most apparent concentration distribution at the *x*-axis position of 500 mm, and the high electromagnetic frequency has a short wavelength, which corresponds to a low penetration depth of electromagnetic as compared with the depth of the porous media as soil. Consequently, the electromagnetic frequency of 2.45 GHz affects the concentration distribution more than the electromagnetic frequency of 4 GHz.

3.4 The Influence of Inlet Concentration of Contaminant in the Porous Media as Soil. The temperature distribution in the porous media as soil at operating inlet concentrations of contaminant $C_{in} = 0.03$ and 30 mol/dm^3 is displayed in Fig. 8. It seems that $C_{in} = 30$ mol/dm^3 expands the temperature distribution on the top edge of porous media further since the inlet concentration of the contaminant is more intense. The determination of the boundary conditions at the upper and lower surface of porous media as soil ($C_H = 20$ mol/dm^3, $C_L = 10$ mol/dm^3) results in the most apparent temperature distribution at the upper location. Since the concentration diffuses from high concentrations to low concentrations, As a result, the contaminant inlet concentration of 30 mol/dm^3 is the most influential factor in temperature distribution.

The velocity patterns of fluid in the porous media as soil inlet concentrations of contaminants C_{in} 0.03 and 30 mol/dm^3 are displayed in Fig. 8. The results show that inlet concentrations of contaminant C_{in} 0.03 mol/dm^3 which have the velocity patterns clearly different, especially in the top area, because the effect of natural convection and electromagnetic waves is greater than the effect of the inlet concentration of contaminant in porous media as soil.

4 Conclusions

In order to investigate the contaminants of groundwater within porous media such as soil, the concentration distribution of the contaminated water is depicted in the presented model. The fundamentals of mass transport through a saturated porous media in the presence of an electromagnetic field were studied. When compared to the available experimental data in the literature, the model predictions showed very good agreement. The electromagnetic field approach to groundwater was used to account for the

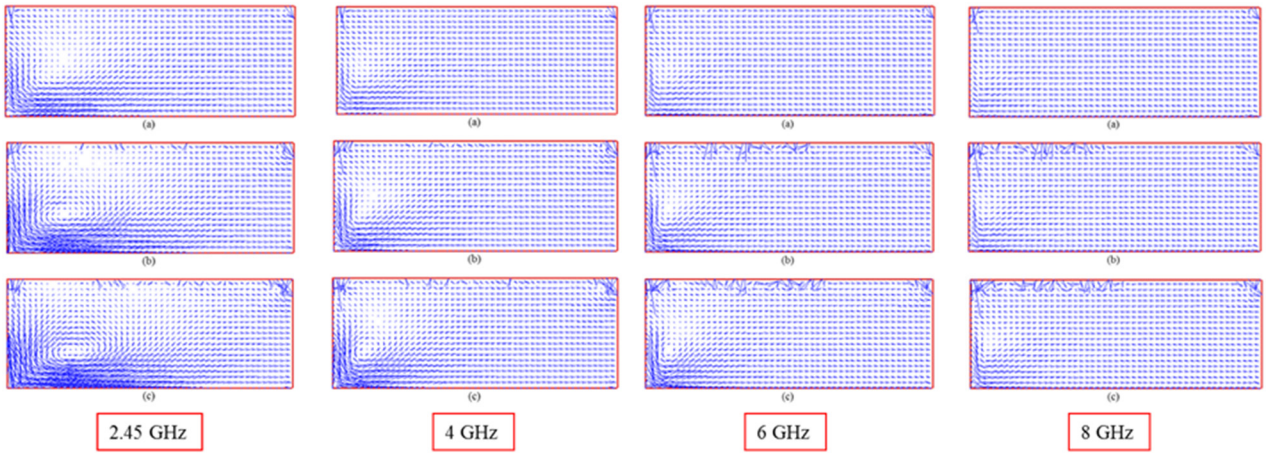

Fig. 6 Velocity patterns when elapsed times (*a*) 20 s, (*b*) 40 s, (*c*) 60 s when varied electromagnetic frequency 2.45, 4, 6 and 8 GHz, respectively (electromagnetic power 1600 W, $Re_p = 0.1$, inlet concentration of contaminant = 30 mol/dm^3)

Table 2 Concentration distribution at various electromagnetic wave frequencies (2.45 and 4 GHz) at *y*-axis 199 mm, Re_p 0.1, inlet concentration of contaminant 30 mol/dm^3 when elapsed time 60 s (electromagnetic power 1600 w)

	Concentration of contaminant (mol/dm^3)	
x-axis (mm)	f 2.45	f 4
1	9.62001	9.61913
5	8.97792	8.97494
15	8.77120	8.77081
55	8.64581	8.63828
95	8.64615	8.63751
135	8.64771	8.63984
175	8.64618	8.64036
215	8.64402	8.64037
255	8.64189	8.64043
295	8.63898	8.64078
335	8.64424	8.64177
375	8.64473	8.64346
415	8.68609	8.68529
455	9.00171	9.00127
495	12.44996	12.44990
500	13.55693	13.55697

effect of frequency and concentration change. Previous research in this area concentrated solely on the electromagnetic field effects on transport through porous media. This model shows that the low electromagnetic frequency (2.45 GHz) has the most influence on the phenomena of heat and mass transport and includes the velocity patterns in the porous media. So, the velocity dissipation increases as the electromagnetic frequency decreases. Moreover, the increasing inlet concentration of contaminants (C_{in} 30 mol/dm^3) has the greatest influence on the temperature distribution during low electromagnetic wave frequency (2.45 GHz). So the temperature distribution increases as the concentration of contaminants increases.

This study helps to indicate guidelines on the effect of the concentrations of contaminants in the soil by analyzing the effects of electromagnetic fields on heat and mass transport through porous media. Electric and magnetic fields have only a minor impact on heat flux distribution, which is consistent with previous research [30]. Finally, the LTNE model is the most reasonable for this case study.

Funding Data

- Program Management Unit for Human Resources & Institutional Development, Research, and Innovation, NXPO (Grant Nos. B05F630092, B05F64020).
- Thailand Science Research and Innovation Fundamental Fund (Project No. 66082).

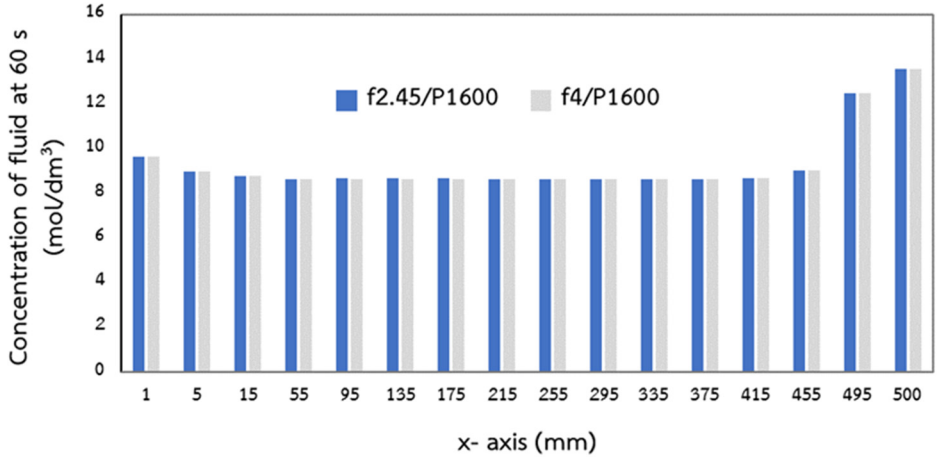

Fig. 7 The bar graph of concentration distribution when elapsed time 60 s along *x*-axis at varied electromagnetic frequency (2.45 GHz and 4 GHz) in the range of *y*-axis is 199 mm (electromagnetic wave power of 1600 w, inlet concentration of contaminant 30 mol/dm^3.)

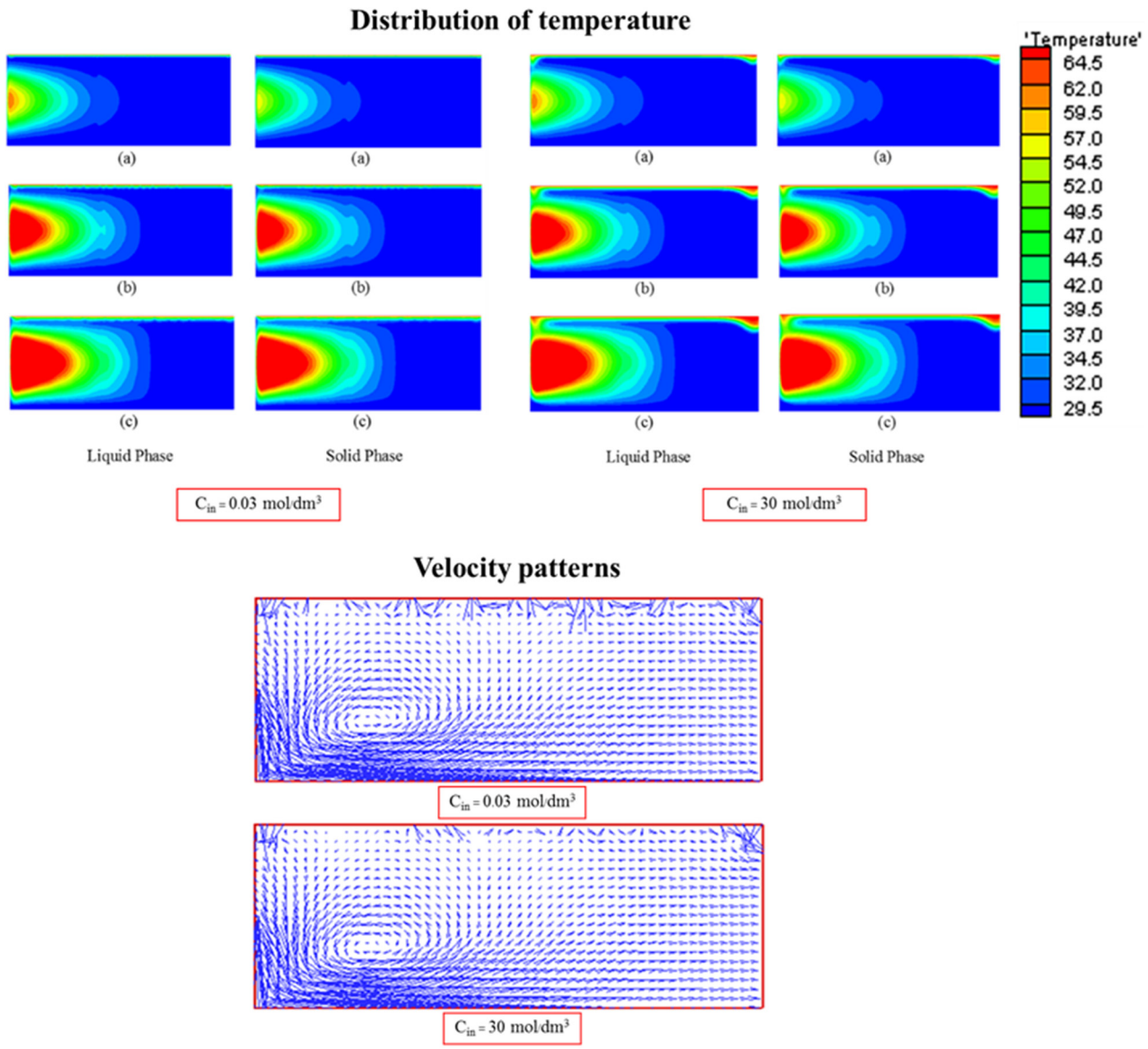

Fig. 8 The temperature distribution in porous media as soil (° C) when elapsed times (*a*)–(*c*) 20, 40, 60 s, respectively, and velocity patterns when elapsed time 60 s on the varied concentration of contaminant under the electromagnetic frequency 2.45 GHz, electromagnetic power 1600 W, Reynolds number (Re_p) 0.1

Nomenclature

A = area (m^2)
C_p = specific heat (J kg^{-1} K^{-1})
D_p = penetration depth (m)
E = electric field (V/m)
f = electromagnetic wave frequency (Hz)
h = heat transfer coefficient (W/m^2 K)
H = magnetic field strength (A/m)
k = thermal conductivity (W m^{-1} K^{-1})
P = power (W)
Q = heat generation term (W/m^3)
Re_p = particle Reynolds number
T = temperature (°C)
T = time (s)
Tanδ = dielectric loss coefficient
v, u = velocity (m/s)

Greek Symbols

β_t = coefficient of thermal expansion
β_c = coefficient of concentration expansion
γ_0 = dielectric constant
γ_r' = relative dielectric constant
γ_r'' = relative dielectric loss factor
ε = porosity
μ = dynamic viscosity (kg $m^{-1}s^{-1}$)
ρ = density (kg m^{-3})
σ = electric conductivity (S m^{-1})
ϕ = magnetic permeability (h/m)
ω = angular frequency (rad/s)

Subscripts

f = fluid
s = solid
x, y, z = coordinate

References

[1] Chatterjee, S., Basak, T., and Das, S. K., 2007, "Microwave Driven Convection in a Rotating Cylindrical Cavity: A Numerical Study," J. Food Eng., **79**(4), pp. 1269–1279.

[2] Khanafer, K., and Vafai, K., 2002, "Double-Diffusive Mixed Convection in a Lid-Driven Enclosure Filled With a Fluid-Saturated Porous Medium," Numer. Heat Transfer, Part A, **42**(5), pp. 465–486.
[3] Montienthong, P., Rattanadecho, P., and Klinbun, W., 2017, "Effect of Electromagnetic Field on Distribution of Temperature, Velocity and Concentration During Saturated Flow in Porous Media Based on Local Thermal Non-Equilibrium Models (Influent of Input Power and Input Velocity)," Int. J. Heat Mass Transfer, **106**, pp. 720–730.
[4] Ayuttaya, S. N., Suwimon, C. C., Rattanadecho, P., and Kreewatcharin, T., 2012, "Effect of Ground Arrangements on Swirling Flow in a Rectangular Duct Subjected to Electrohydrodynamic Effects," ASME J. Fluids Eng., **135**(5), p. 051211.
[5] Pengpom, N., Vongpradubchai, S., and Rattanadecho, P., 2019, "Numerical Analysis of Pollutant Concentration Dispersion and Convective Flow in a Two-Dimensional Confluent River Model," Math. Modell. Eng. Probl., **6**(2), pp. 271–279.
[6] Jena, S. K., Mahapatra, S. K., and Sarkar, A., 2013, "Double Diffusive Buoyancy Opposed Natural Convection in a Porous Cavity Having Partially Active Vertical Walls," Int. J. Heat Mass Transfer, **62**, pp. 805–817.
[7] Trevisan, Osvair, and Adrian Bejan. "Mass and Heat Transfer by High Rayleigh Number Convection in a Porous Medium Heated From belowTransfert de Masse Par Convection Thermique a Grand Nombre de Rayleigh Dans un Milieu Poreux Chauffe Par le basStofftransport Durch Natürliche Konvektion Bei Hohe," Int. J. Heat Mass Transfer **30**(11), pp. 2341–2356.
[8] Prasad, V., and Tuntomo, A., 1987, "Inertia Effects on Natural Convection in a Vertical Porous Cavity," Numer. Heat Transfer, **11**(3), pp. 295–320.
[9] Rattanadecho, P., Aokiand, K., and Akahori, M., October 2002, "Experimental Validation of a Combined Electromagnetic and Thermal Model for a Microwave Heating of Multi-Layered Materials Using a Rectangular Wave Guide," ASME J. Heat Transfer-Trans. ASME, **124**(5), pp. 992–996.
[10] Ratanadecho, P., Aoki, K., and Akahori, M., Feb 2002, "Influence of Irradiation Time, Particle Sizes, and Initial Moisture Content During Microwave Drying of Multi-Layered Capillary Porous Materials," ASME J. Heat Transfer-Trans. ASME, **124**(1), pp. 151–161.
[11] Yousefi, Tara, S.A. Mousavi, M.Z. Saghir, and B. Farahbakhsh. "An Investigation on the Microwave Heating of Flowing Water: A Numerical Study," Int. J. Therm. Sci. **71**: pp. 118–127.
[12] Serttikul, C., Datta, A. K., and Rattanadecho, P., 2019, "Effect of Layer Arrangement on 2-D Numerical Analysis of Freezing Process in Double Layer Porous Packed Bed," Int. J. Heat Technol., **37**(1), pp. 273–284.
[13] Wessapan, T., and Rattanadecho, P., 2014, "Influence of Ambient Temperature on Heat Transfer in the Human Eye During Exposure to Electromagnetic Fields at 900 MHz," Int. J. Heat Mass Transfer, **70**, pp. 378–388.
[14] Klinbun, W., Rattanadecho, P., and Pakdee, W., 2011, "Microwave Heating of Saturated Packed Bed Using a Rectangular Waveguide (TE_{10} Mode): Influence of Particle Size, Sample Dimension, Frequency, and Placement Inside the Guide," Int. J. Heat Mass Transfer, **54**(9–10), pp. 1763–1774.
[15] Wessapan, T., and Rattanadecho, P., 2016, "Flow and Heat Transfer in Biological Tissue Due to Electromagnetic Near-Field Exposure Effects," Int. J. Heat Mass Transfer, **97**, pp. 174–184.
[16] Ayuttaya, S. N., Suwimon, C. C., and Rattanadecho, P., 2013, "Numerical Analysis of Electric Force Influence on Heat Transfer in a Channel Flow (Theory Based on Saturated Porous Medium Approach)," Int. J. Heat Mass Transfer, **64**, pp. 361–374.
[17] Makul, N., Rattanadecho, P., and Agrawal, D. K., 2014, "Applications of Microwave Energy in Cement and Concrete – A Review," Renewable Sustainable Energy Rev., **37**, pp. 715–733.
[18] Keangin, P., Vafai, K., and Rattanadecho, P., 2013, "Electromagnetic Field Effects on Biological Materials," Int. J. Heat Mass Transfer, **65**, pp. 389–399.
[19] Belmiloudi, A., 2010, "Parameter Identification Problems and Analysis of the Impact of Porous Media in Biofluid Heat Transfer in Biological Tissues During Thermal Therapy," Nonlinear Anal.: Real World Appl., **11**(3), pp. 1345–1363.
[20] Afrin, N., Zhang, Y., and Chen, J. K., 2011, "Thermal Lagging in Living Biological Tissue Based on Nonequilibrium Heat Transfer Between Tissue, Arterial and Venous Bloods," Int. J. Heat Mass Transfer, **54**(11–12), pp. 2419–2426.
[21] Klinbun, W., Vafai, K., and Rattanadecho, P., 2012, "Electromagnetic Field Effects on Transport Through Porous Media," Int. J. Heat Mass Transfer, **55**(1–3), pp. 325–335.
[22] Wessapan, T., and Rattanadecho, P., 2020, "Acoustic Streaming Effect on Flow and Heat Transfer in Porous Tissue During Exposure to Focused Ultrasound," Case Stud. Therm. Eng., **21**, p. 100670.
[23] Amiri, A., and Vafai, K., 1994, "Analysis of Dispersion Effects and Non-Thermal Equilibrium, Non-Darcian, Variable Porosity Incompressible Flow Through Porous Media," Int. J. Heat Mass Transfer, **37**(6), pp. 939–954.
[24] Montienthong, P., and Rattanadecho, P., 2019, "Focused Ultrasound Ablation for the Treatment of Patients With Localized Deformed Breast Cancer: Computer Simulation," ASME J. Heat Transfer-Trans. ASME, **141**(10), p. 101101.
[25] Mahmoudi, Y., and Maerefat, M., 2011, "Analytical Investigation of Heat Transfer Enhancement in a Channel Partially Filled With a Porous Material Under Local Thermal Non-Equilibrium Condition," Int. J. Therm. Sci., **50**(12), pp. 2386–2401.
[26] Khalid, A., Khan, I., Khan, A., Shafie, S., and Tlili, I., 2018, "Case Study of MHD Blood Flow in a Porous Medium With CNTS and Thermal Analysis," Case Stud. Therm. Eng., **12**, pp. 374–380.
[27] Preechaphonkul, W., and Rattanadecho, P., 2021, "The Comparative of the Performance for Predicted Thermal Models During Microwave Ablation Process Using a Slot Antenna," Case Stud. Therm. Eng., **25**, p. 100908.
[28] Sorokin, K. E., and Perepechko, Y. V., 2021, "Thermal Convection of Fluid-Saturated Granular Medium in Acoustic Field," Int. J. Numer. Methods Fluids, **93**(2), pp. 339–355.
[29] Rattanadecho, P., Makul, N., Pichaicherd, A., Chanamai, P., and Rungroungdouyboon, B., 2016, "A Novel Rapid Microwave-Thermal Process for Accelerated Curing of Concrete: Prototype Design, Optimal Process and Experimental Investigations," Constr. Build. Mater., **123**(1), pp. 768–784.
[30] Elmaboud, Y., Abdelsalam, S. I., Mekheimer, K., and Vafai, K., 2019, "Electromagnetic Flow for Two-Layer Immiscible Fluids," Eng. Sci. Technol. Int. J., **22**(1), pp. 237–248.
[31] Wang, S., Vafai, K., and Mukhopadhyay, S., 2014, "Two-Phase CO_2 Migration in Tilted Aquifers in the Presence of Groundwater Flow," Int. J. Heat Mass Transfer, **77**, pp. 717–729.
[32] Shafahi, M., and Vafai, K., 2011, "Interfacial Interactions of Biomaterials in Water Decontamination Applications," J. Mater. Sci., **46**(19), pp. 6277–6284.
[33] Mur, G., 1981, "Absorbing Boundary Conditions for the Finite Difference Approximation of the Time-Domain Electromagnetic-Field Equations," IEEE Trans. Electromagn. Compat., **EMC-23**(4), pp. 377–382.
[34] Rattanadecho, P., and Klinbun, W., 2012, "Numerical Analysis of Natural Convection in Porous Media Subjected to Electromagnetic Energy Using Local Thermal Nonequilibrium (LTNE) Models," Drying Technol. Int. J., **30**(16), pp. 1896–1905.